
Supplementary information

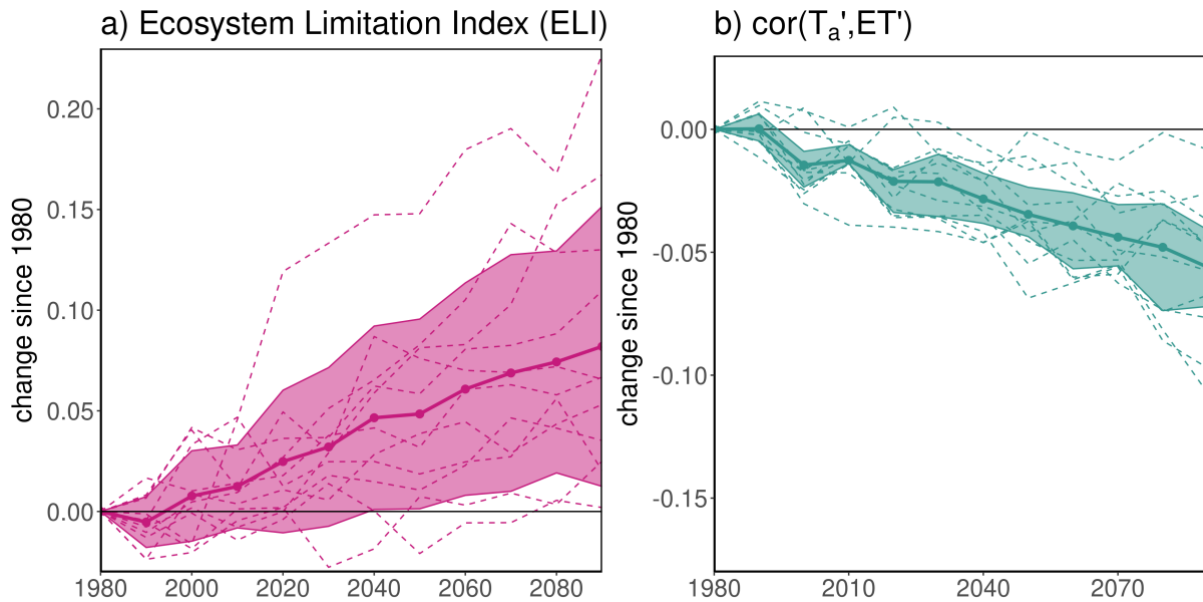
Widespread shift from ecosystem energy to water limitation with climate change

In the format provided by the authors and unedited

1 **Supplementary material**

2 **Figures**

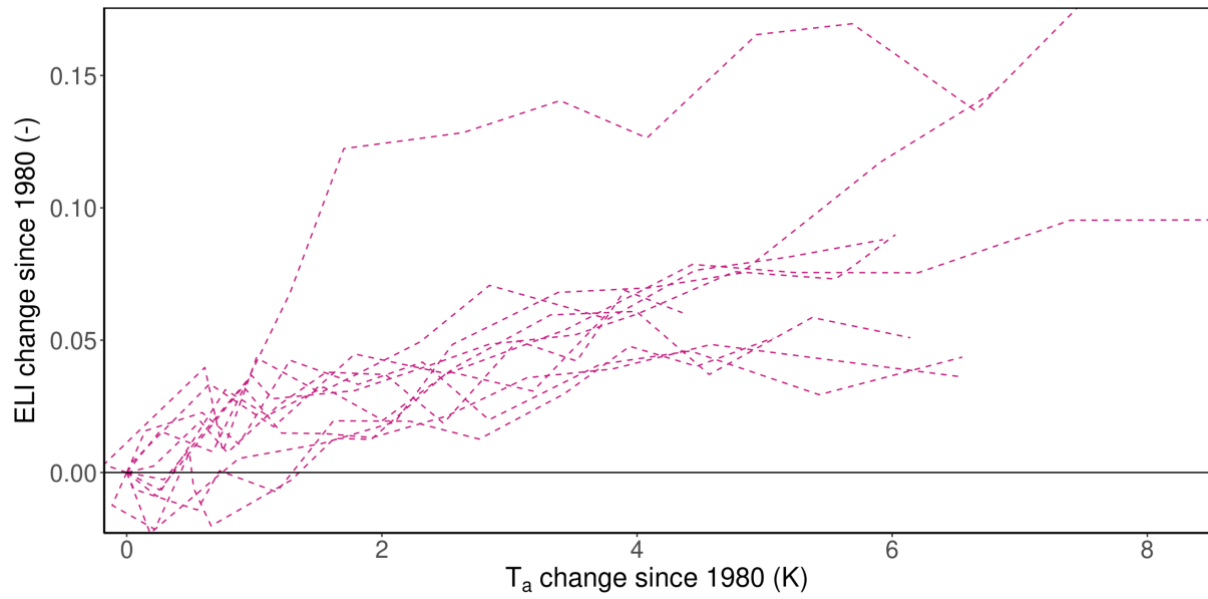
3 All figures are created with the ggplot2 package and, if applicable, the country borders using
4 the maptools package^{1,2}.



5

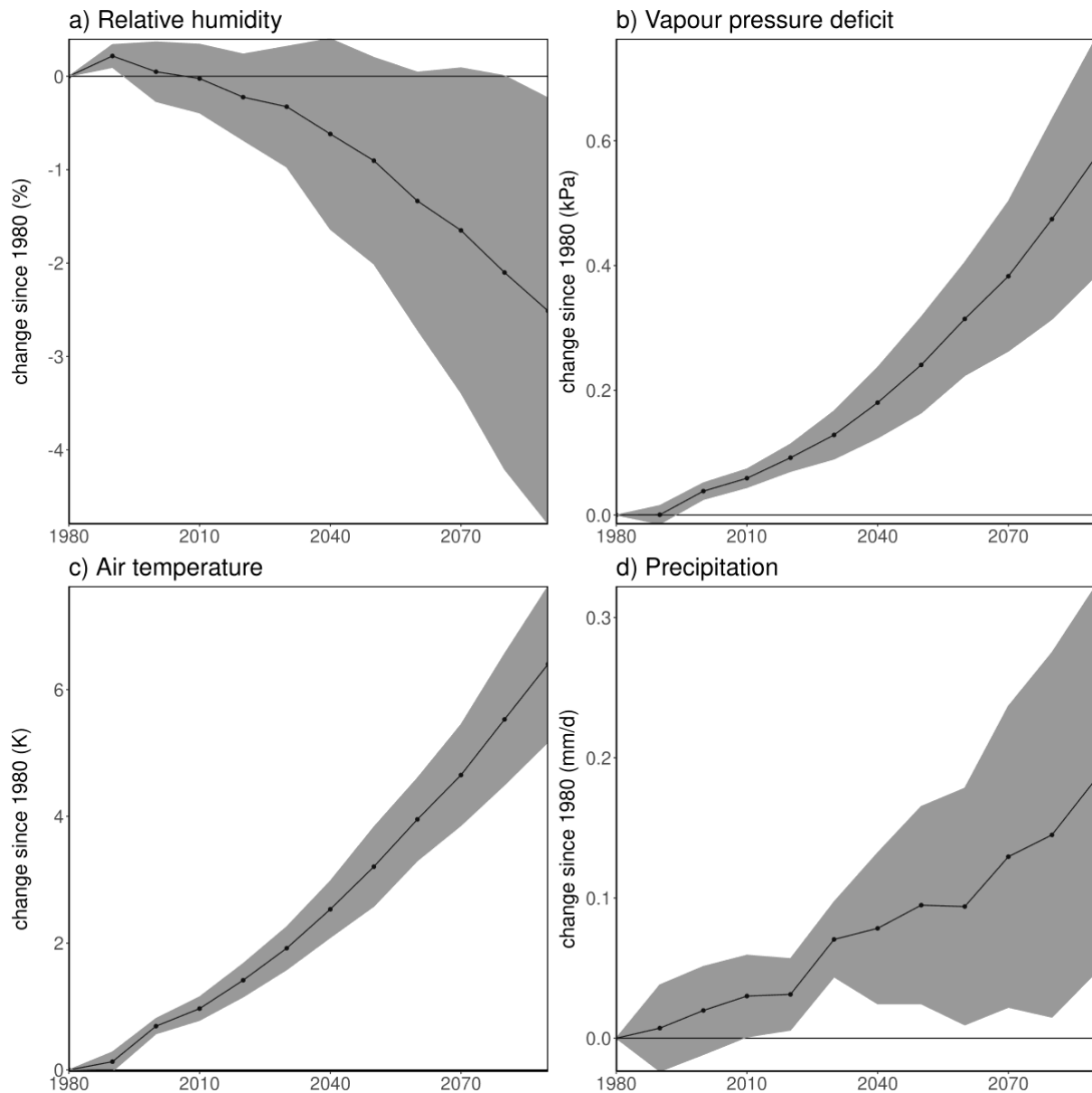
6 **Supplementary figure 1: a) Past and projected global trends in ELI based on air**
7 **temperature anomalies and b) cor(T_a',ET')**. Dashed colored lines depict the globally and
8 decadal average time series of all respective variables per individual model. Solid lines with
9 dots depict multi-model mean time series inferred from the model-specific time series, where
10 the shaded regions cover +/- 1 multi-model standard deviation. The y-axis denotes the change
11 since 1980 in respective units. Global averages are calculated over land grid cells that have
12 complete time series for all models and variables and are weighted according to the surface area
13 per grid cell.

14



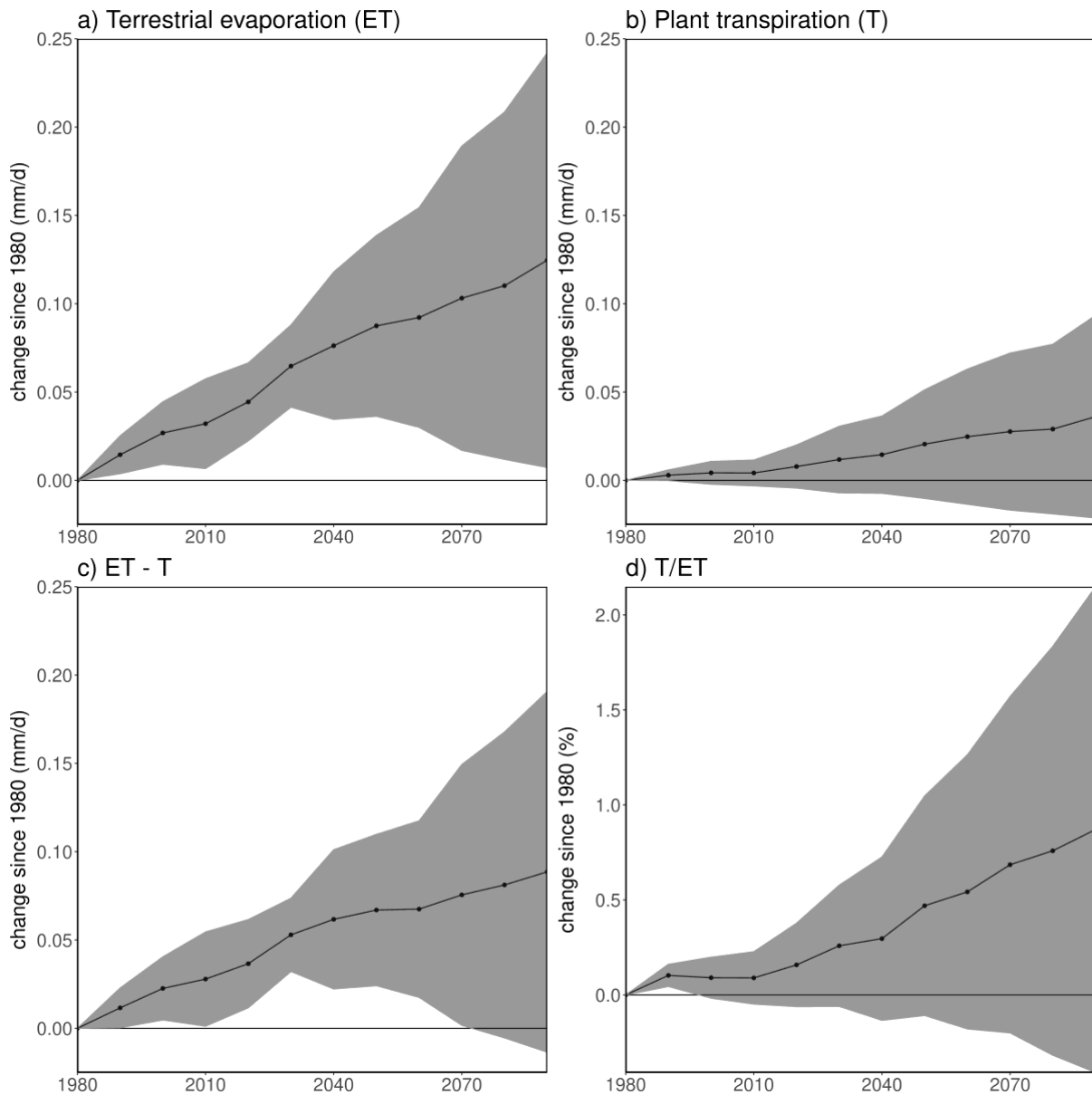
15

16 **Supplementary Figure 2: Past and projected global trends in ELI for model-specific air**
17 **temperature warming levels. Dashed colored lines depict the globally and decadal average**
18 **time series of ELI per individual model.**



19

20 **Supplementary figure 3: Past and projected global climate trends.** Global trends of a)
 21 relative humidity, b) vapour pressure deficit, c) air temperature and d) precipitation from 1980
 22 - 2100 for 7 models only (Methods). Solid lines with dots depict the multi-model mean time
 23 series of the respective variables inferred from model-specific globally and decadal averaged
 24 time series, where the shaded regions cover ± 1 multi-model standard deviation. The y-axis
 25 denotes the change since 1980 in respective units. Global averages are calculated over land grid
 26 cells that have complete time series for all models and variables and are weighted according to
 27 the surface area per grid cell.



29

30 **Supplementary figure 4: Past and projected global trends of evaporative components.**

31 Global trends of a) terrestrial evaporation, b) plant transpiration (Methods), c) ET – T,

32 effectively the sum of bare soil evaporation and canopy interception, d) fraction plant transpired

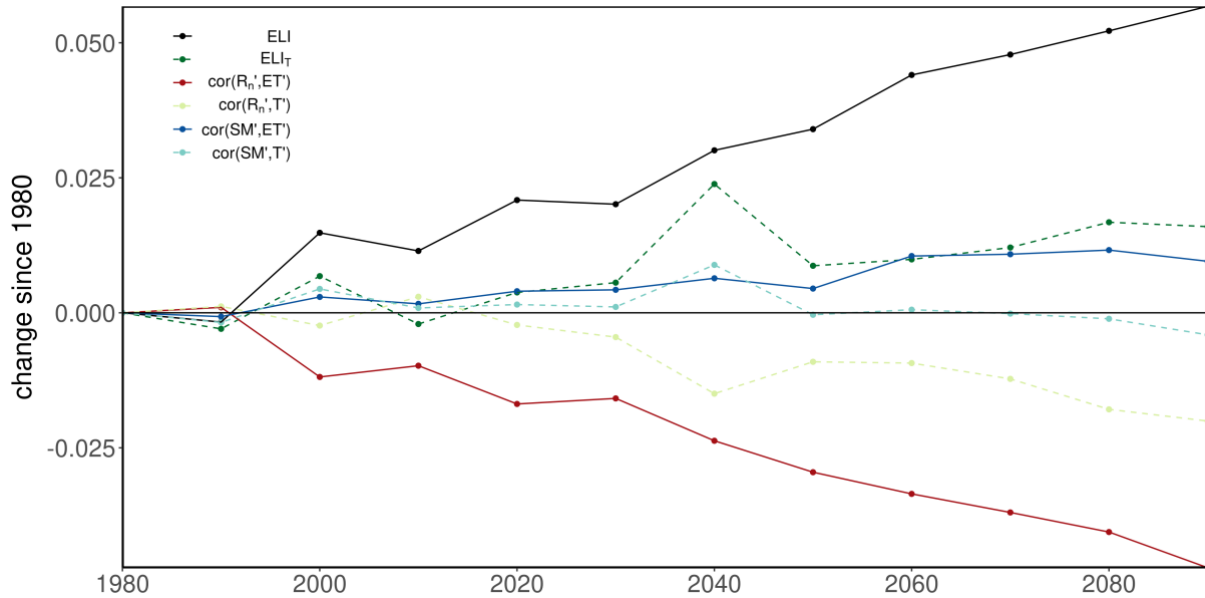
33 water (plant transpiration over terrestrial evaporation) from 1980 - 2100 for 7 models only

34 (Methods). Solid lines with dots depict the multi-model mean time series of the respective

35 variables inferred from model-specific globally and decadal averaged time series, where the

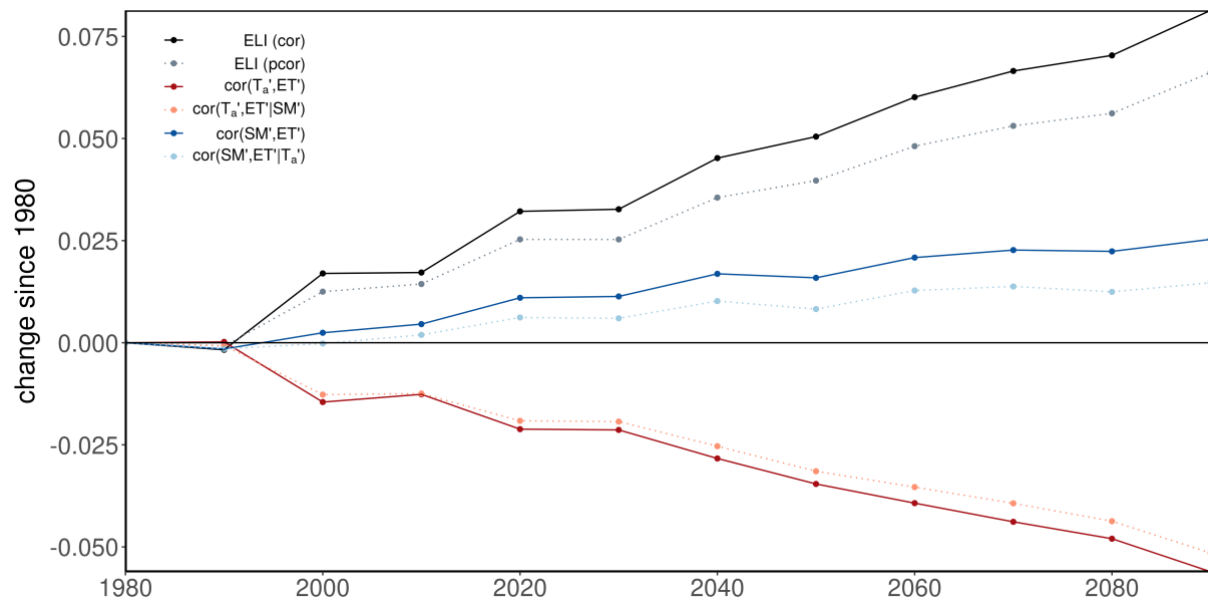
36 shaded regions cover +/- 1 multi-model standard deviation. The y-axis denotes the change since

37 1980 in respective units. Global averages are calculated over land grid cells that have complete
38 time series for all models and variables and are weighted according to the surface area per grid
39 cell.



40

41 **Supplementary figure 5: Global trends of Ecosystem Water Limitation Index and its**
42 **individual components with terrestrial evaporation and transpiration for 7 models only**
43 **(Methods)**. Individual components consist of the correlation between anomalies of either
44 surface net radiation (R_n) or soil moisture (SM) with either terrestrial evaporation (solid lines)
45 or transpiration (dashed lines). Global averages are calculated over land grid cells that have
46 complete time series for all models and variables and are weighted according to the surface area
47 per grid cell. Solid and dashed lines with dots depict the multi-model mean time series of the
48 variables displayed in the legend inferred from model-specific globally and decadal averaged
49 time series, where the shaded regions cover +/- 1 multi-model standard deviation. All y-axes
50 denote changes since 1980.



51

52

53 **Supplementary figure 6: Confounding effects of energy on water control and vice versa**

54 **on the Ecosystem Water Limitation Index and its individual components. Solid and dotted**

55 **lines with dots depict the multi-model mean time series of the variables displayed in the legend**

56 **inferred from model-specific globally and decadal averaged time series, where the shaded**

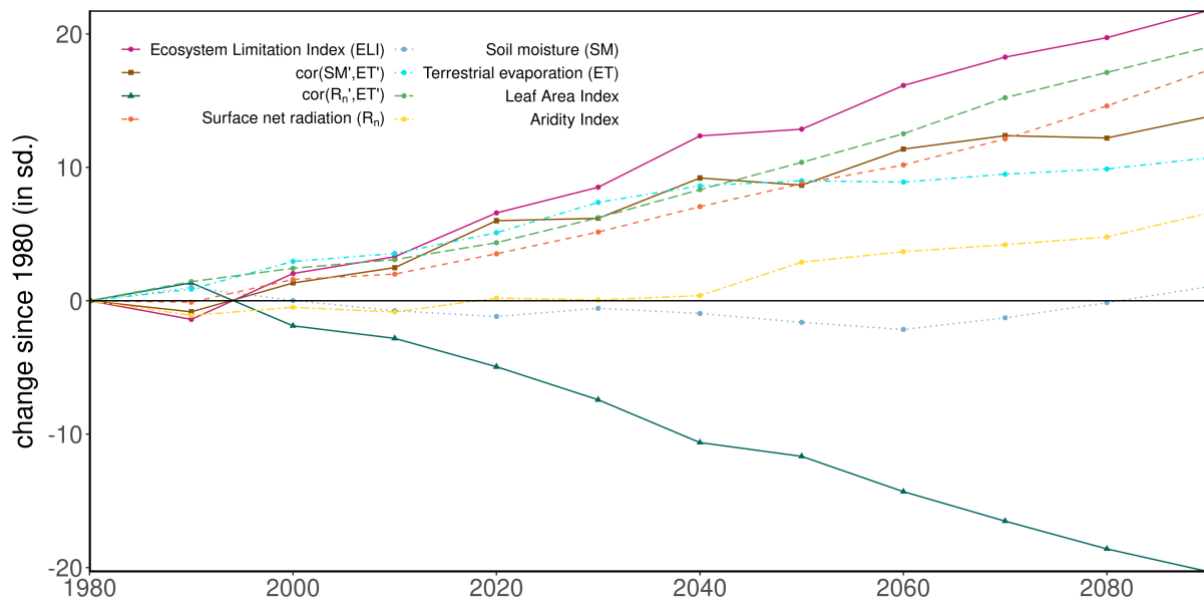
57 **regions cover +/- 1 multi-model standard deviation. Global averages are calculated over land**

58 **grid cells that have complete time series for all models and variables and are weighted according**

59 **to the surface area per grid cell. Solid lines with dots are the ELI from Figure 1a) (black) and**

60 **components (red, blue), where the dotted lines with dots are the ELI based on partial**

61 **correlations. All y-axes denote changes since 1980.**



62

63 **Supplementary figure 7: Past and projected global climate and vegetation trends**

64 **normalized by natural variability (standard deviation of respective detrended decadal**

65 **time series per variable; solid dotted lines).** Solid lines with dots denote ELI and its individual

66 components, the other line types denote other variables displayed in the legend. All lines with

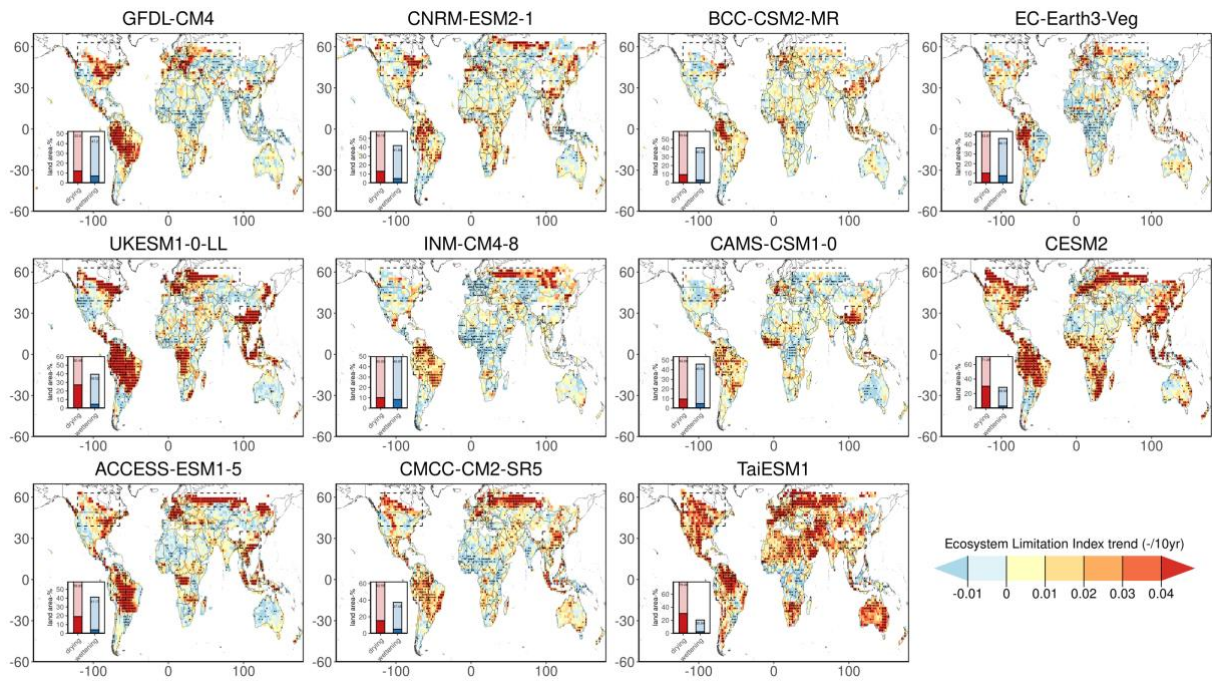
67 dots depict the multi-model mean time series of the variables displayed in the legend inferred

68 from model-specific globally and decadal averaged time series. The y-axis denotes the change

69 since 1980 in standard deviations (sd). Global averages are calculated over land grid cells that

70 have complete time series for all models and variables and are weighted according to the surface

71 area per grid cell.

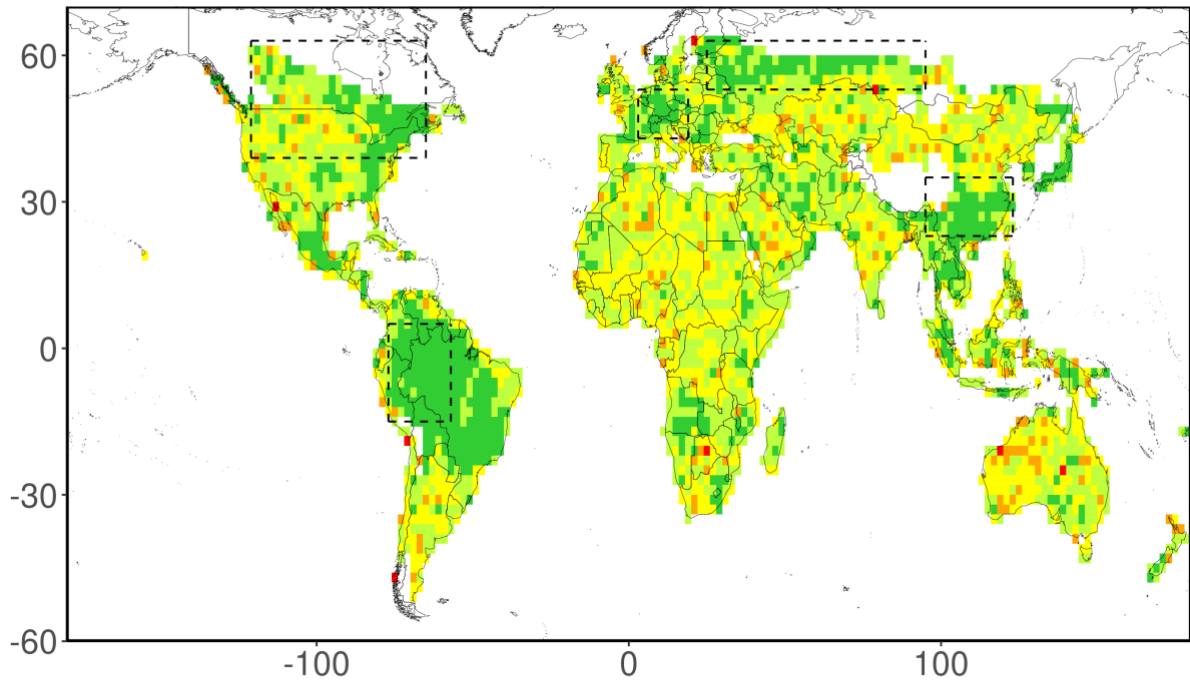


72

73

74 **Supplementary figure 8: Ecosystem Water Limitation Index trends calculated per**
 75 **individual model.** The trend in the multi-model mean time series of ELI (dots indicate
 76 significance: $p < 0.05$) is based on Kendall's tau statistic. The dashed boxes indicate regions of
 77 interest. The inset displays the fraction of the warm land area that is drying or wettening
 78 according to ELI trends.

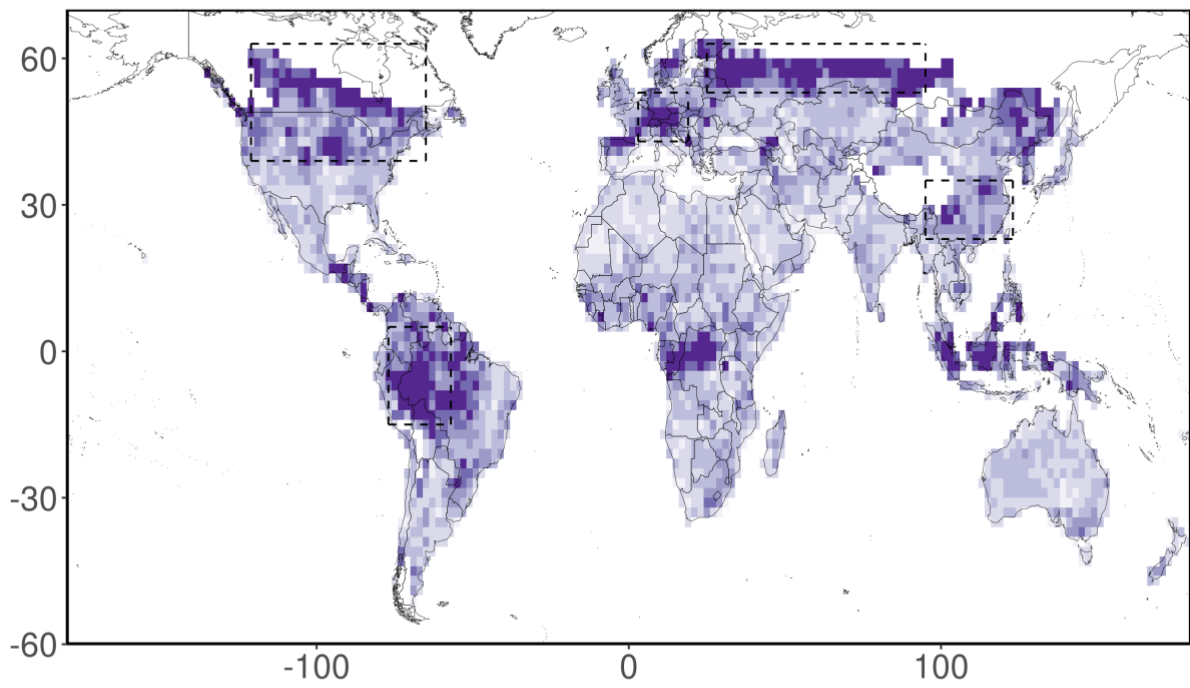
a)



Agreement on multi-model mean ELI trend sign (%)

0 20 40 60 80 100

b)

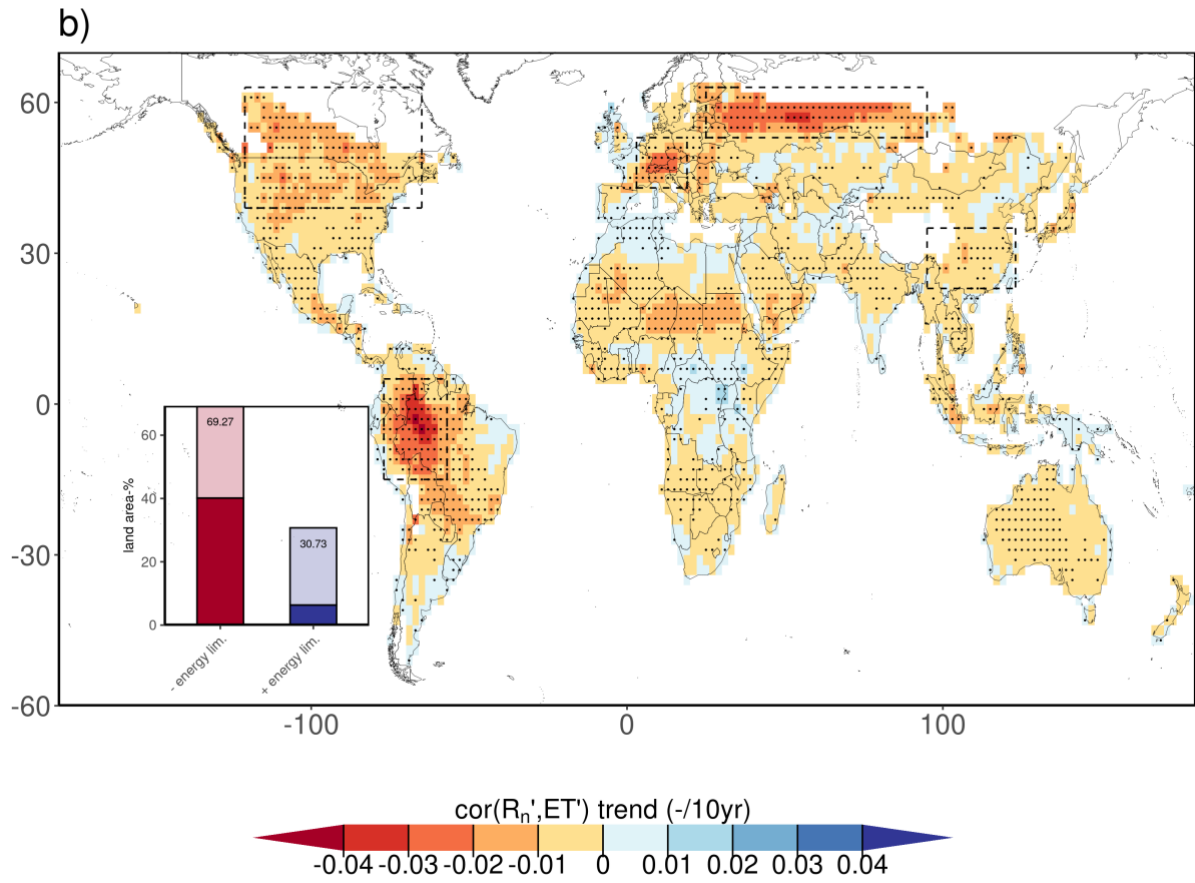
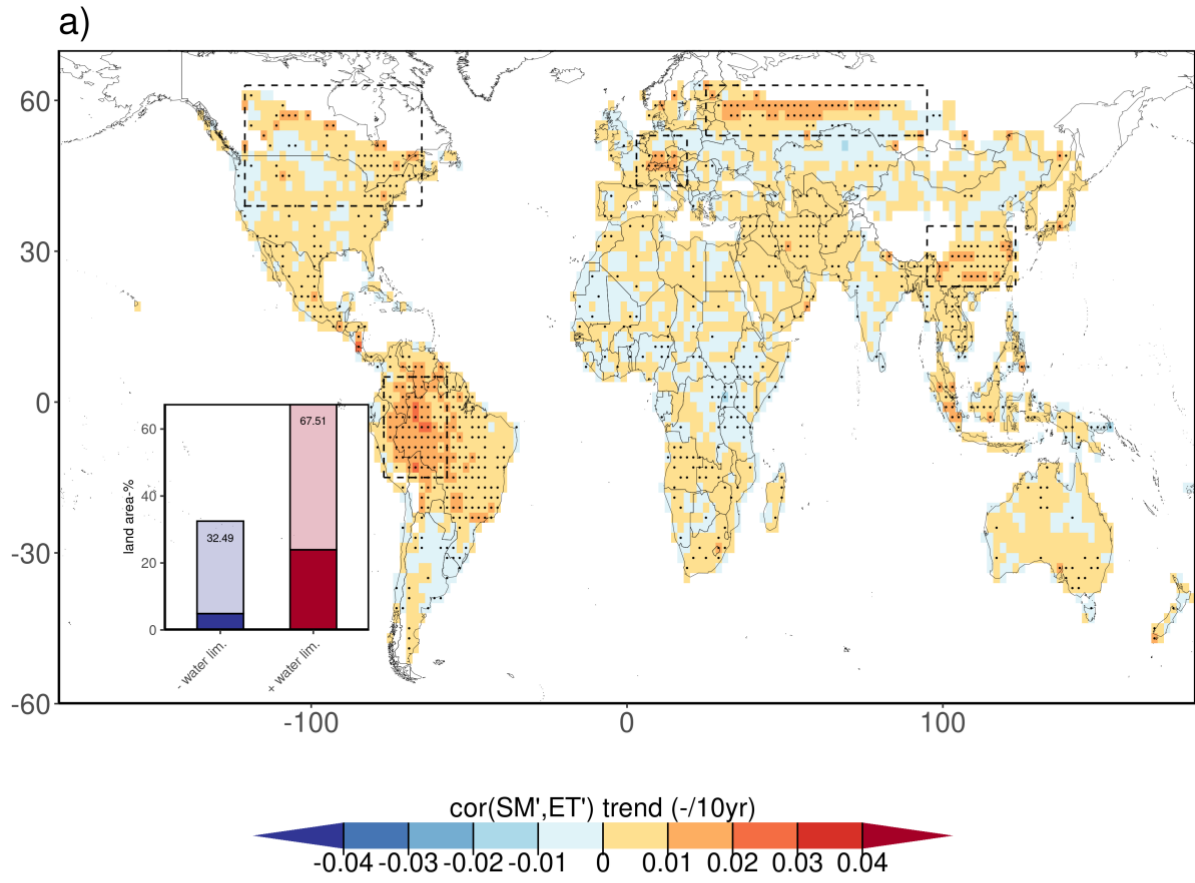


σ_{ELI} between individual slopes

0.01 0.015 0.02 0.025 0.03

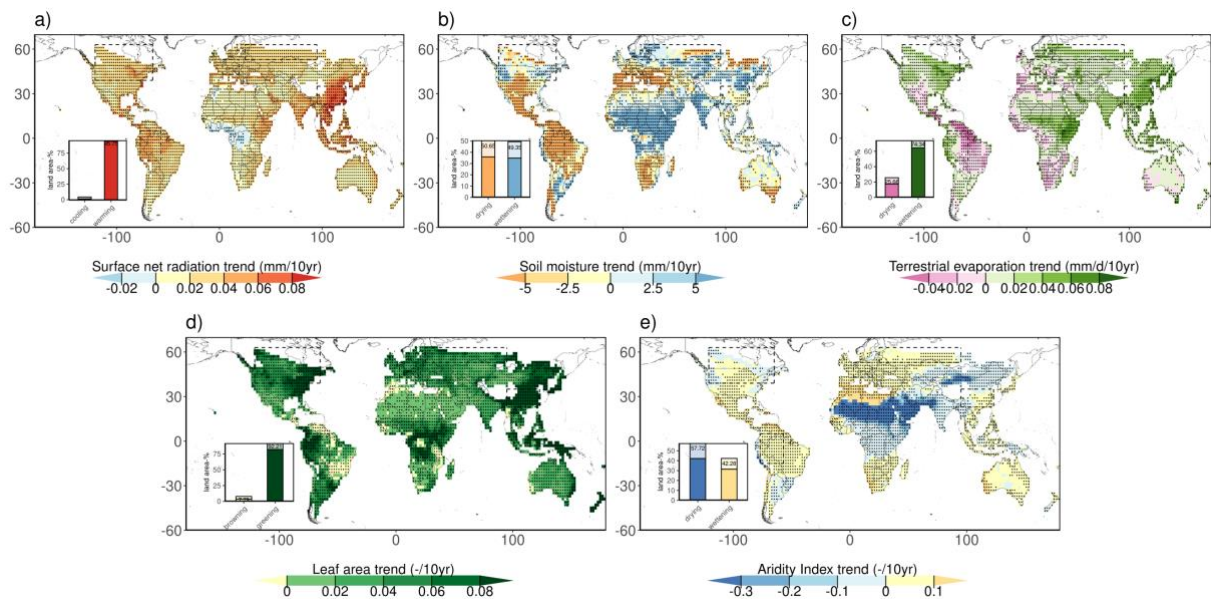
80

81 **Supplementary figure 9: Comparison between trends of individual CMIP6 models from**
82 **1980 - 2100 (Supplementary figure 5).** a) The percentage of models (from models that actually
83 have a value in the respective grid cell) for which their respective ELI trends agree with the
84 sign of the multi-model mean (Figure 2a). b) The standard deviation (σ_{ELI}) between individual
85 slopes of CMIP6 models (Supplementary figure 4).



87

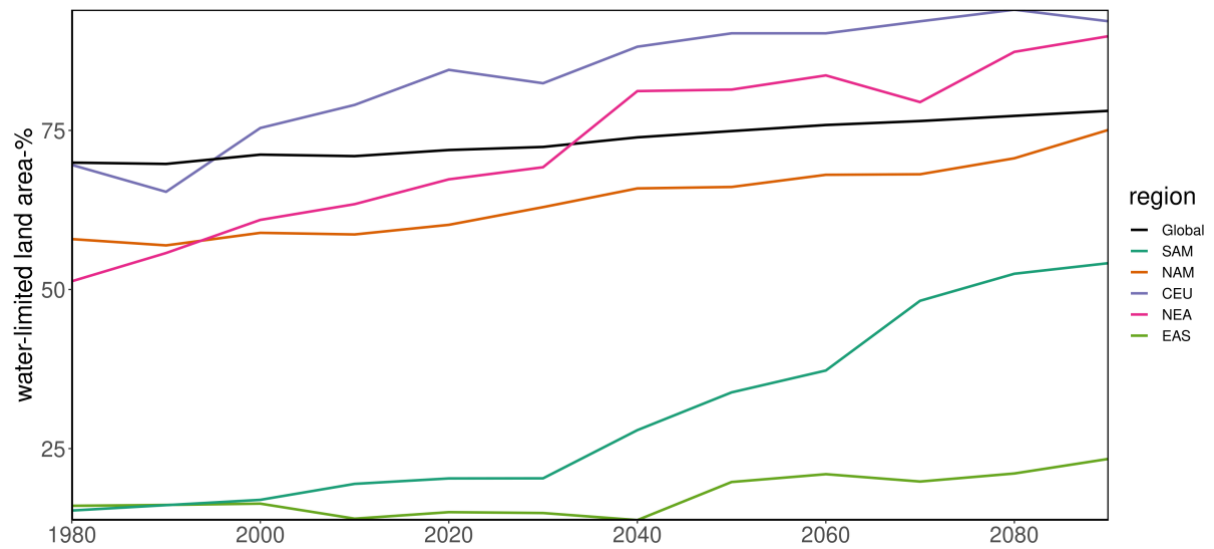
88 **Supplementary figure 10: Mapping of the trends of individual components of ELI,**
89 **$\text{cor}(\text{SM}',\text{ET}')$ (a) and $\text{cor}(\text{R}_n',\text{ET}')$ (b) from 1980 to 2100.** The trends are based on Kendall's
90 tau statistic (dots indicate significance: $p < 0.05$). The dashed boxes indicate regions of interest.
91 Inset plots display the fraction of warm land area with a decrease or increase in energy or water
92 control ($p < 0.05$ is hued darker).



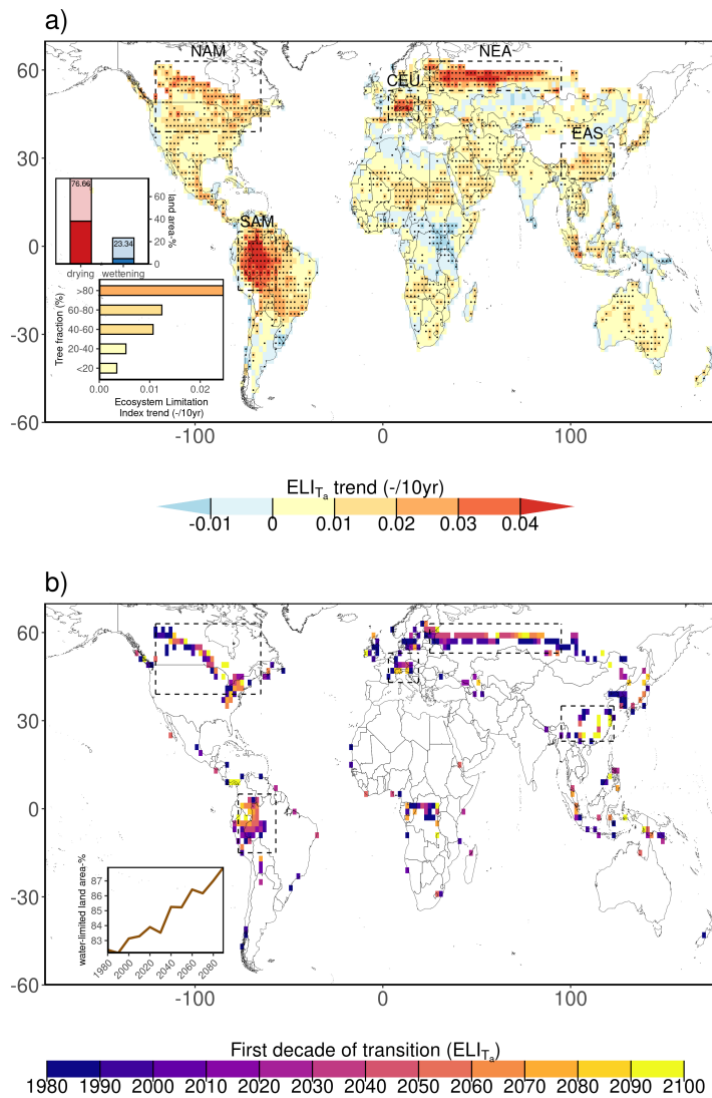
93

94

95 **Supplementary figure 11: Trends based on multi-model mean time series of land-**
96 **atmosphere variables from 1980 to 2100.** The trends are based on Kendall's tau statistic (dots
97 indicate significance: $p < 0.05$). The dashed boxes indicate regions of interest. Inset plots
98 display the fraction of warm land area with negative or positive trends of all respective variables
99 ($p < 0.05$ is hued darker).



100
 101 **Supplementary Figure 12: Trends in water-limited area fraction across the globe and**
 102 **regions of interest.** Colored lines depict the globally and decadal average time series of
 103 water-limited fraction of the warm land area, averaged over all individual models.



104

105 **Supplementary Figure 13: Global distribution and trends of ecosystem water limitation**

106 **derived with air temperature (T_a) instead of surface net radiation anomalies. a) Trend in**

107 **the multi-model mean of ELI (dots indicate significance: $p < 0.05$ based on Kendall's tau**

108 **statistic). The dashed boxes indicate regions of interest, which allow easier cross-comparisons**

109 **with other maps. The top inset displays the fraction of the warm land area that is drying or**

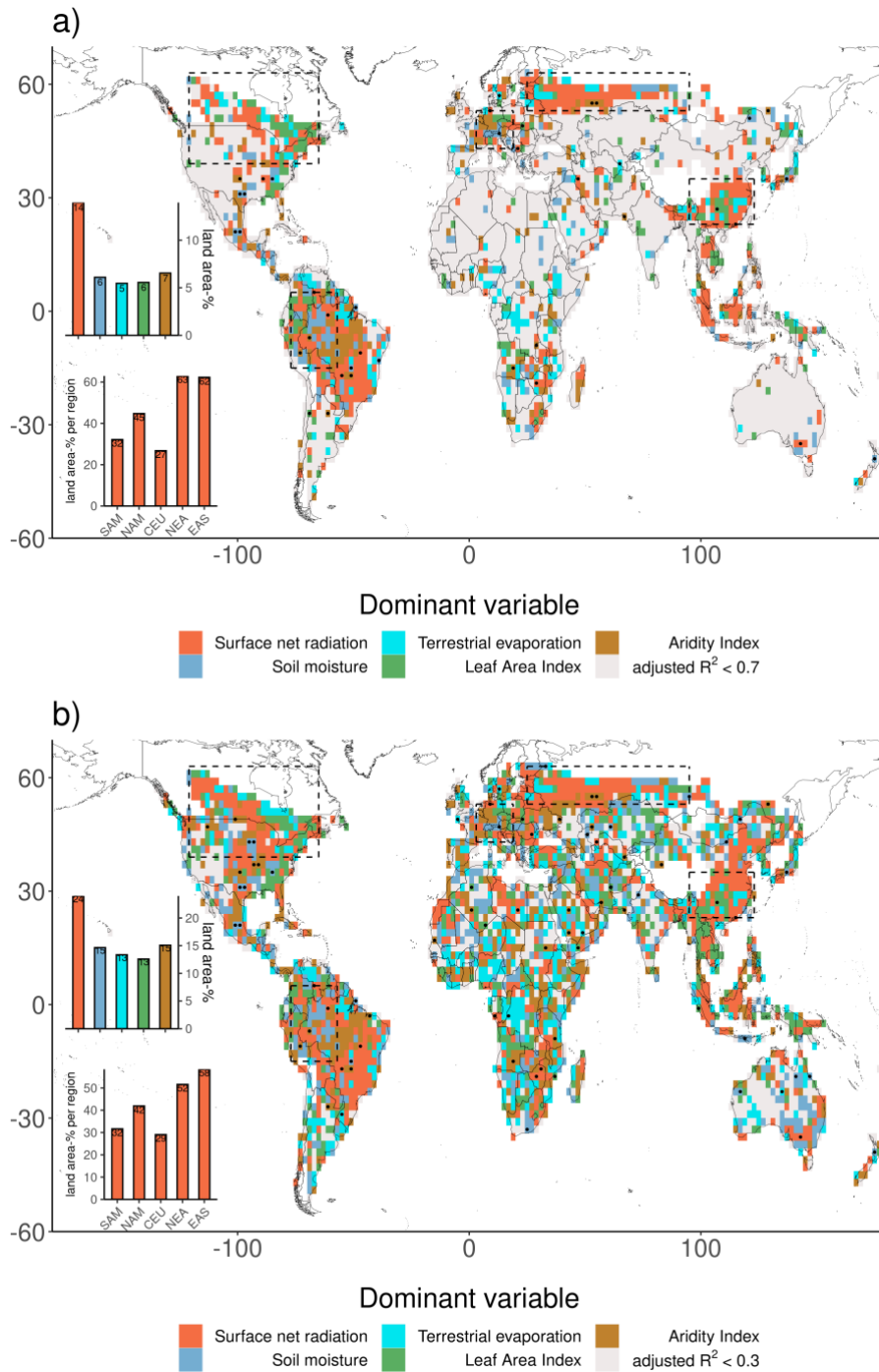
110 **wetting according to ELI trends ($p < 0.05$ is hues darker). The bottom inset displays area-**

111 **weighted average ELI trends for regions with different tree fractions based on 6 CMIP6 models**

112 **(Methods). b) Timing of regime shift from energy to water limitation as indicated by ELI values**

113 **becoming positive. The inset shows the global time series of the water-limited fraction of the**

114 **warm land area (Methods).**



115

116 **Supplementary figure 14: Attribution of ELI trends to land-atmosphere variables with**

117 **different thresholds for explanatory power of the multiple linear models. Adjusted $R^2 >$**

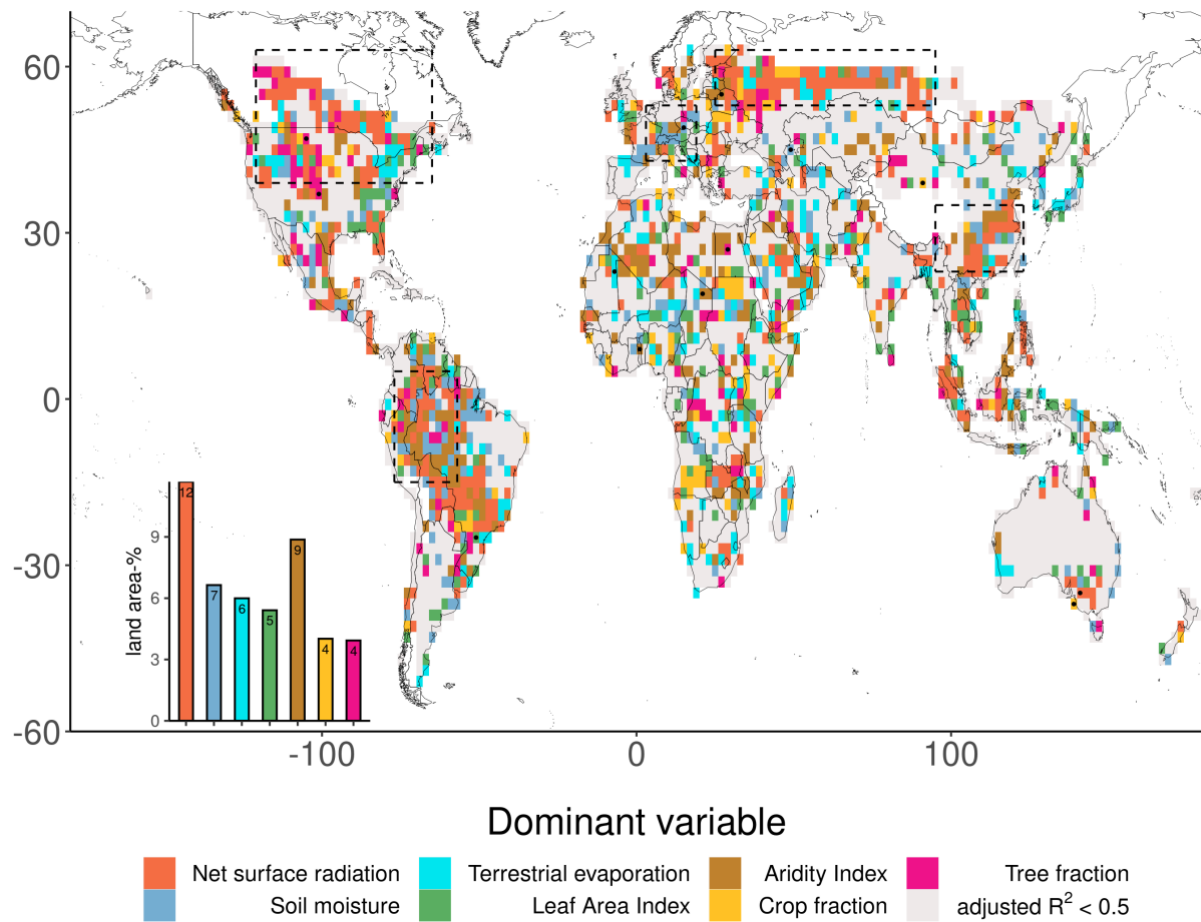
118 **0.7 a) and adjusted $R^2 > 0.3$ b). Colors indicate the variables that best predict the decadal ELI**

119 **dynamics calculated using multivariate linear regression with a set of equally well-performing**

120 **models, across which the most meaningful predictor is selected (Methods). Stippling indicates**

121 **grid cells where only one linear model performs well (exceeding the respective adjusted R^2**

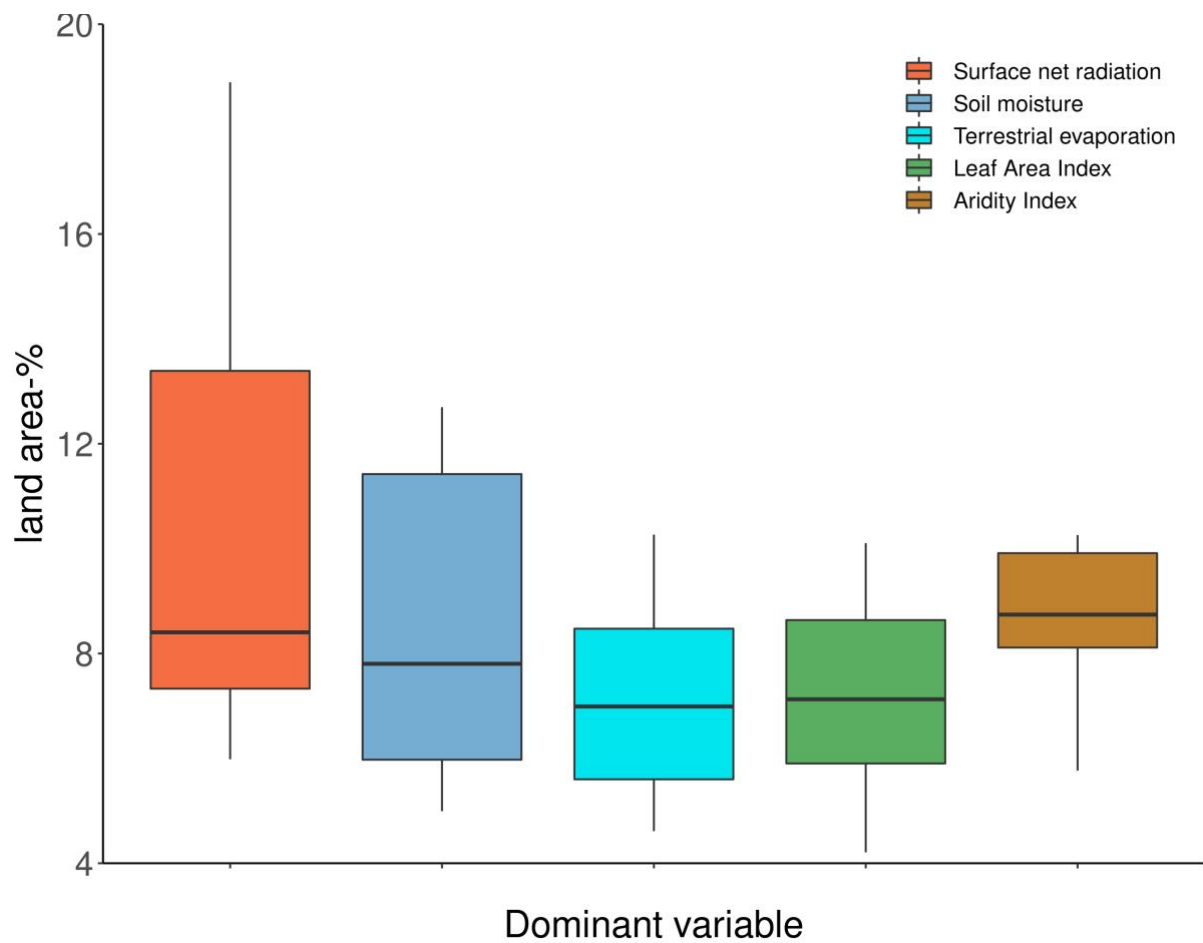
122 threshold) and contains only a single explanatory variable. Grey color denotes grid cells without
 123 any model with reliable performance (not exceeding the respective adjusted R^2 threshold). Inset
 124 plots indicate the total fraction of warm land area controlled by respective variables (top) and
 125 the fraction of ELI trends controlled by surface net radiation per region of interest.



126

127 **Supplementary figure 15: Attribution of ELI trends to land-atmosphere variables**
 128 **including proxies for land use change, crop and tree fraction (for 6 CMIP6 models only;**
 129 **Methods).** Dots indicate that there is only one linear model that is significant (adjusted $R^2 >$
 130 0.5) and contains only one single explanatory variable, and grey warm land area lacking any
 131 significant multivariate linear model (adjusted $R^2 < 0.5$). Inset plots indicate the total fraction

132 of warm land area governed by respective variables.



133

134

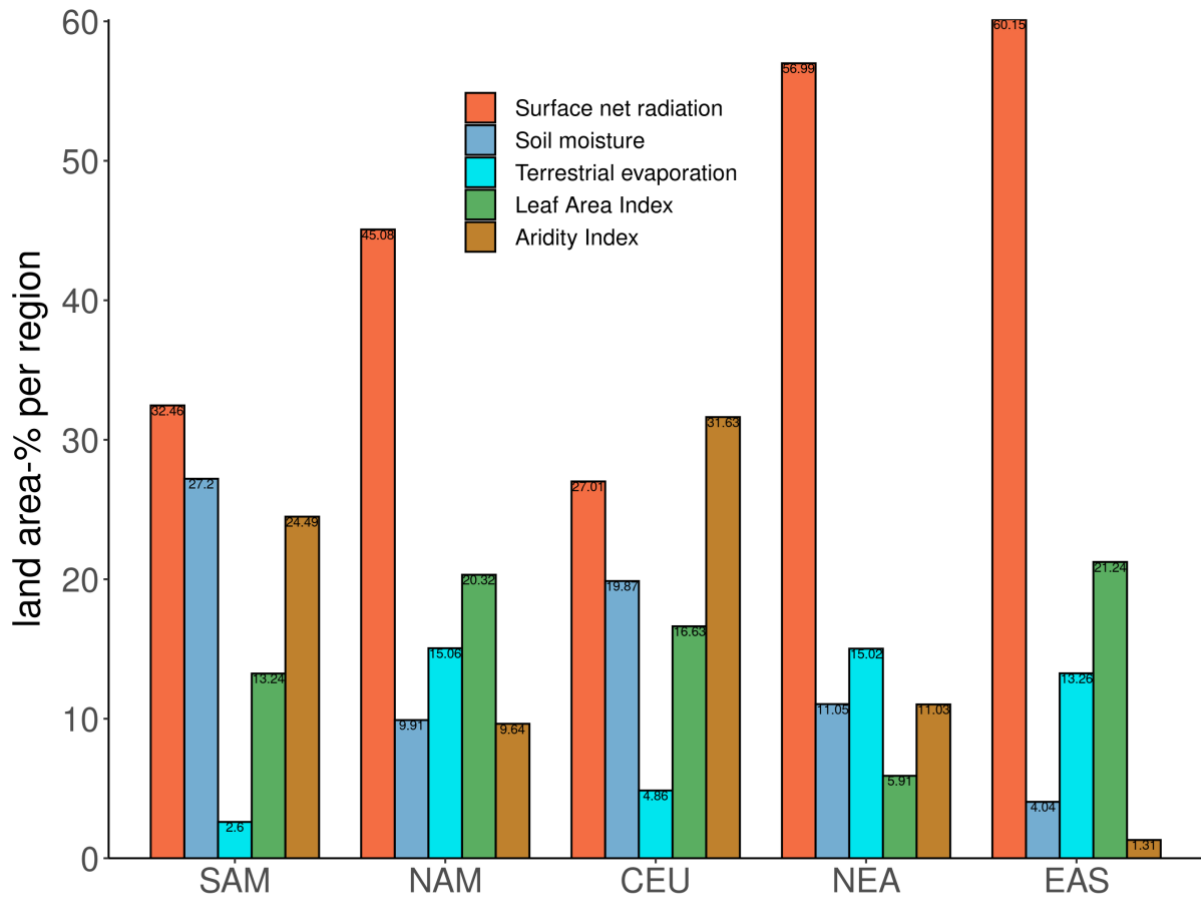
135 **Supplementary figure 16: The importance of land-atmosphere variables per CMIP6**

136 **model.** Area fraction of grid cells with adjusted $R^2 > 0.5$ that is governed by a respective

137 variable. Box-and-whisker plots display the median (horizontal bar), 25th and 75th percentiles

138 (hinges) and largest and smallest values that do not exceed 1.5 * of the inter-quartile range.

139



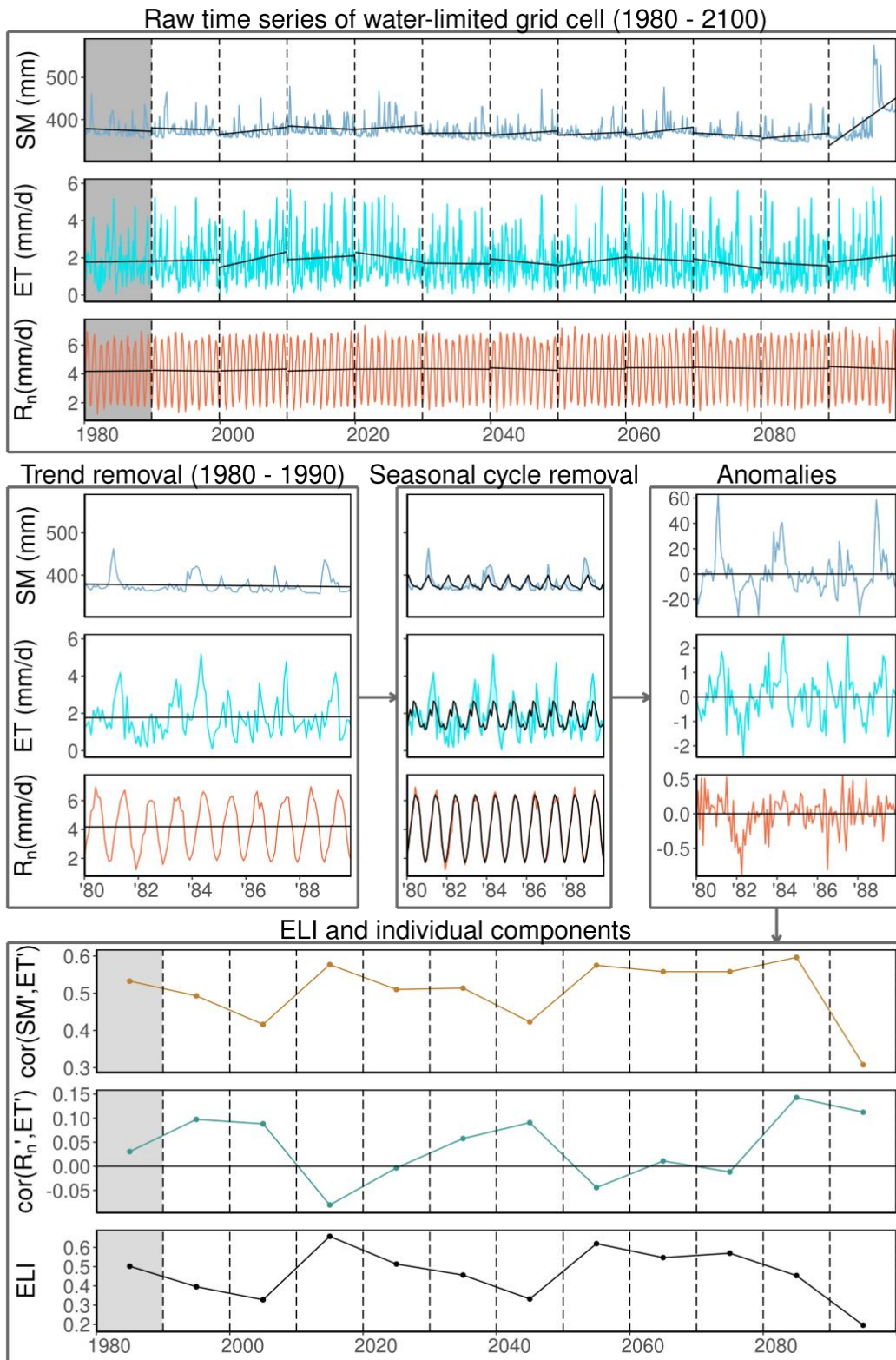
140

141 **Supplementary figure 17: The importance of land-atmosphere variables per region of**

142 **interest.** Area fraction of grid cells within regions of interest with adjusted $R^2 > 0.5$ that is

143 governed by a respective variable.

144



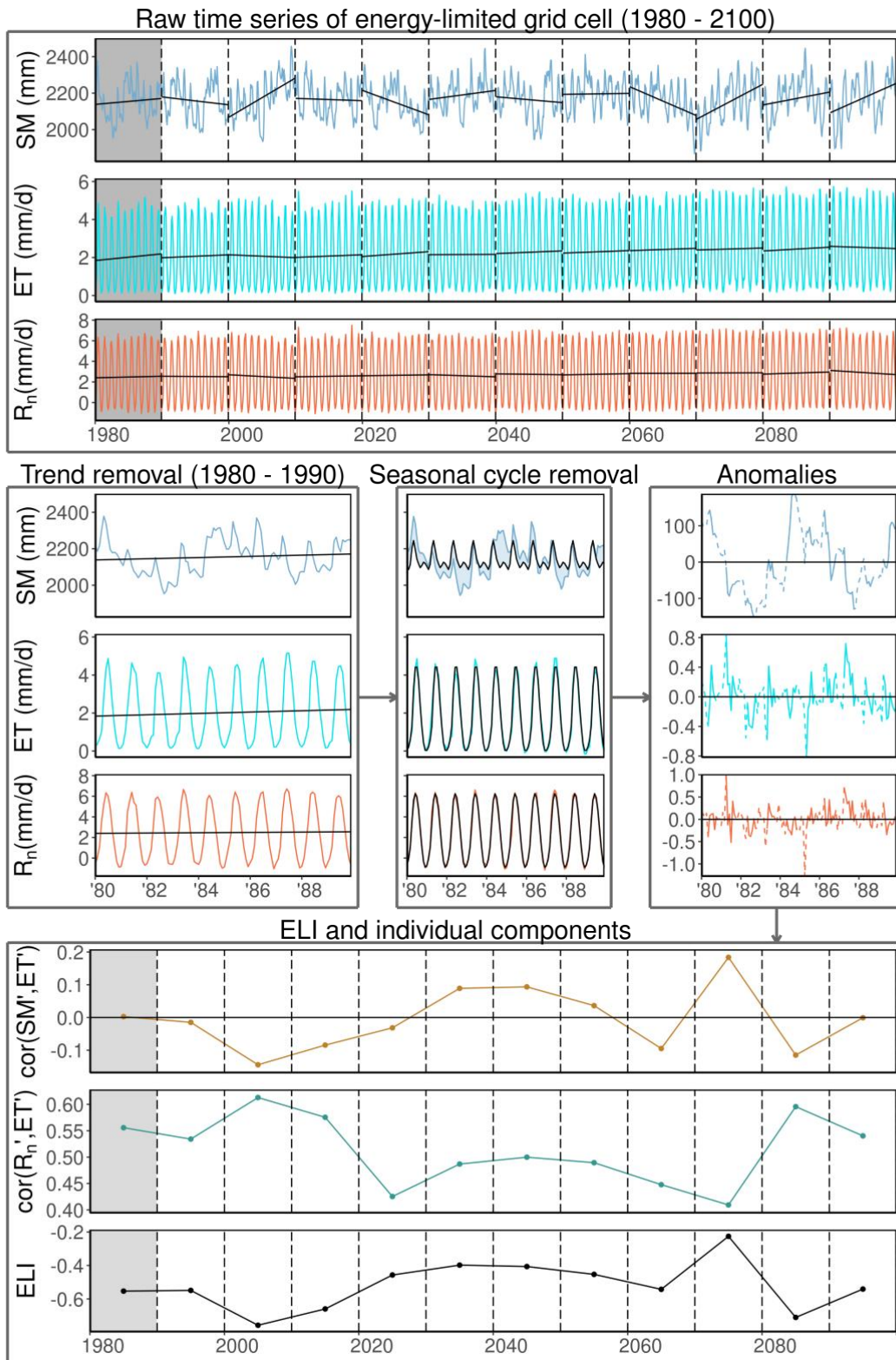
145

146 **Supplementary figure 18: Illustration of procedure of computing the ELI in a water-**

147 **limited example grid cell (29° N and 101° W).** The colored lines in the top panel show, from

148 top to bottom, the raw time series for the 120-year study period for soil moisture (SM),

149 terrestrial evaporation (ET) and surface net radiation (R_n). Vertical dashed lines separate the
150 time series into decades, within which we determined the linear trends (black solid lines) we
151 use for detrending. The grey shading indicates the decade that we use to illustrate the
152 computation of the monthly anomalies. The left panel in the middle row shows the same as the
153 top panel, but just for 1980-1990. The middle panel in the middle row shows the detrended time
154 series (colored lines) imposed on the seasonal cycle (black), revealing the monthly anomalies
155 (shaded region between colored and black lines). The colored lines in the right panel in the
156 middle row show the anomalies, where dashed lines indicate monthly temperatures colder than
157 10 °C. Only the data in months with temperature exceeding 10 °C (solid lines) are used to
158 compute the correlations that constitute the ELI. The bottom panel shows, from top to bottom,
159 $\text{cor}(SM', ET')$, $\text{cor}(R_n', ET')$ and the ELI. The arrows in the figure indicate step-wise
160 computation of the ELI. All results are from the INM-CM4-8 model (Supplementary table 3).



161

162 **Supplementary figure 19: Similar to Supplementary Figure 17 but for an energy-limited**

163 **example grid cell (49° N and 75° W).**

164

165 ***Validation of ELI with conceptual model***

166 Our motivation for the application of ELI to indicate water- versus energy-limited conditions
167 was explained in the introduction. Here, we establish the ability of ELI to reflect water-limited
168 conditions by using a conceptual soil moisture model, which is forced by the potential ET (ET_p)
169 and precipitation, and computes actual ET, leakage from the root-zone ($Q_{leakage}$) and soil
170 moisture (SM). The actual ET is computed as a function of ET_p and SM, as follows:

171 (1) $ET = ET_p * \beta_{SM}$

172 where the soil moisture stress function (β_{SM}) can be defined with three linear relationships:

173 (2)
$$\beta_{SM} = \begin{cases} 0 & \text{if } SM < SM_{wilt} \\ \frac{SM - SM_{wilt}}{SM_{crit} - SM_{wilt}} & \text{if } SM_{wilt} < SM < SM_{crit} \\ 1 & \text{if } SM_{crit} < SM < SM_{sat} \end{cases}$$

174 where SM_{wilt} is the wilting point, SM_{crit} the critical soil moisture and SM_{sat} the soil moisture
175 content at saturation. Soil parameters were adopted from the HTESSSEL model ($SM_{wilt} = 0.171$,
176 $SM_{crit} = 0.323$ and $SM_{sat} = 0.472$). ET_p is computed using a simplification of the Priestley-Taylor
177 method (as previously done by Lofgren et al.³, Milly and Dunne⁴ and Maes et al.⁵):

178 (3) $ET_p = \alpha_{MD} * R_n$

179 Here, ET_p is assumed to be a fraction ($\alpha_{MD} = 0.8$) of the surface net radiation. The $Q_{leakage}$ is
180 based on Clapp and Hornberger⁶ and Buitink et al.⁷:

181 (4)
$$Q_{leakage} = LSM_t - LSM_{sat} \left[\left(\frac{SM_t}{SM_{sat}} \right)^{-2b-2} + \frac{(2b+2)k_s \Delta t}{SM_{sat} L} \right]^{-\frac{1}{2b+2}}$$

182 where L denotes the rooting depth (1000mm), SM_t the soil moisture content at time t, k_s is the
183 hydraulic conductivity (50mm/d), Δt is the length of time step and b an empirical constant
184 (taken as 5.39). Using Eqs. 1-4, the root-zone soil moisture is prognosed by solving the water
185 balance, as follows:

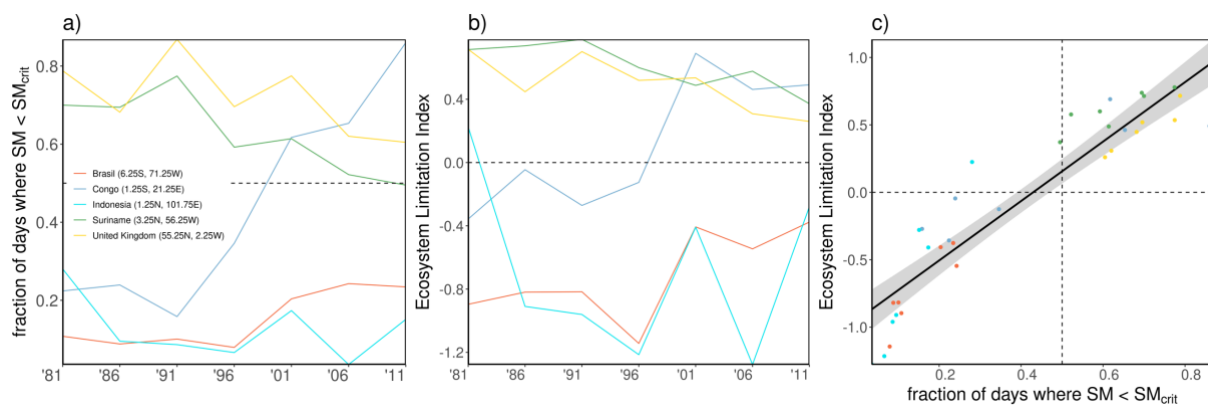
186 (5) $SM_{t+1} = SM_t + \frac{1}{L} (P - ET - Q_{leakage})$

187 where P is total precipitation. The concept of water limitation is straightforward through the
 188 implementation of the soil moisture stress function in Eq. (2) in the model, which renders this
 189 model suitable to validate the ability of ELI to reflect water limited conditions. In climate
 190 models, water limitation is more complex as it is related to several interacting processes and
 191 resulting complex soil moisture stress functions are not readily available as model output,
 192 warranting the application of a more descriptive index, such as the ELI. Here, we define an
 193 index that computes the fraction of days where water-limited conditions prevail (when $SM <$
 194 SM_{crit} , although it should be noted that this is just one definition of water limitation used here
 195 for illustration only).

196

197 We solve this set of equations using surface net radiation and total precipitation from ERA5 at
 198 the daily time scale at a 0.5 x 0.5 degree grid cell resolution from 1981-2016^{8,9}. The fraction of
 199 days where $SM < SM_{crit}$ is computed for every 5-year time interval. In concert, the ELI is
 200 computed as described in the Methods section. We modify this methodology by computing the
 201 ELI i) with the net radiation from ERA5 that is used as model input and the soil moisture and
 202 terrestrial evaporation directly computed by the conceptual model (Equations (1) and (4)) and
 203 ii) for every 5-year time interval to obtain a reasonable time sample, excluding data where there
 204 are fewer than 15 data points with temperatures above 10°C.

205



206

207 **Supplementary Figure 20: Validation of the ability of ELI to reflect water-limited**
 208 **conditions.** Time series of a) fraction of days where $SM < SM_{crit}$ and b) ELI and c) fraction of
 209 days where $SM < SM_{crit}$ versus ELI with data from the conceptual model (points). The solid
 210 black line in c) denotes a linear regression with a 95% confidence interval. Colors denote
 211 different grid cells, selected across the globe and different climate regimes. Conditions above
 212 and right of the dashed lines are assumed water-limited.

213
 214 Time series of the fraction of days where $SM < SM_{crit}$ and the ELI are shown in Supplementary
 215 Figure 20a and b for a number of grid cells distributed across the globe. Note that grid cells
 216 have been selected to reflect a wide range of average climate conditions; from energy- to water-
 217 limited conditions. The order of the time series in both panels are similar, suggesting
 218 comparable spatial variability between the two indices. Further, all grid cells show ample
 219 temporal variability; Whereas the magnitude of the temporal variability is not as
 220 straightforward to compare between a) and b), the sign of the changes in time of both indices
 221 match well. Also, the high correlation between ELI and the conceptual water balance estimates
 222 of water limitation shown in Supplementary Figure 20c confirms the similarity between these
 223 two indices and validates, at least for this selection of grid cells, that the ELI is able to reflect
 224 water-limited conditions.

225

226 **Tables**

227 **Supplementary table 1: Conceptual typical behavior of ELI ($\text{cor}(SM',ET')$ - $\text{cor}(R_n',ET')$)**
 228 **and its individual components $\text{cor}(SM',ET')$ and $\text{cor}(R_n',ET')$ across soil moisture**
 229 **regimes.**

	$SM < SM_{wilt}$	$SM_{wilt} < SM < SM_{crit}$	$SM > SM_{crit}$

Regime	dry	water limitation	energy limitation
$\text{cor}(\text{SM}', \text{ET}')$	≈ 0	> 0	< 0 or ≈ 0
$\text{cor}(\text{R}_n', \text{ET}')$	≈ 0	< 0 or ≈ 0	> 0
ELI	≈ 0	> 0	< 0

230

231 **Supplementary table 2: Overview of signs of individual correlations of the ELI typically**
232 **associated with water and energy-limited conditions, respectively.** All values denote the
233 median of model-specific area fraction of water-limited or energy-limited warm land area that
234 satisfies the combinations; within brackets the interquartile range.

water limitation (ELI > 0)	energy limitation (ELI < 0)
$\text{cor}(\text{SM}', \text{ET}') > 0$ & $\text{cor}(\text{R}_n', \text{ET}') < 0$: 84% (7)	$\text{cor}(\text{SM}', \text{ET}') < 0$ & $\text{cor}(\text{R}_n', \text{ET}') > 0$: 58% (10)
$\text{cor}(\text{SM}', \text{ET}') > 0$ & $\text{cor}(\text{R}_n', \text{ET}') > 0$: 15% (5)	$\text{cor}(\text{SM}', \text{ET}') > 0$ & $\text{cor}(\text{R}_n', \text{ET}') > 0$: 40% (10)

235

236 **Supplementary table 3: An overview of the CMIP6 models used in this study.** For all
237 models, variables temperature (tas), root-zone soil moisture (mrso), terrestrial evaporation
238 (hfls), Leaf Area Index (lai), precipitation (pr) and in- and outgoing short- and longwave
239 radiation (rlds,rsds,rlus,rsus) have been downloaded; here, all variables are abbreviated
240 according to CMIP6 standardized names. *models that additionally provide variables
241 evaporation from the canopy (evspsblveg) and near-surface relative humidity (hurs). **models
242 that additionally provide variables crop fraction (cropFrac) and tree fraction (treeFrac).
243 ***CAMS-CSM1-0 does not contain output for the year 2100, which is copied from 2099, and
244 TaiESM1 does not contain data from December 2100, which is copied from November 2099.
245 Dynamic vegetation reflects whether or not plant functional traits (PFT) can vary in time,

246 responding to competition for resources. However, the resources considered in this context vary
 247 between models.

Institution	Model	Member	Version	Dynamic vegetation	Citation
National oceanic and Atmospheric Administratio n (NOAA), Geophysical Fluid Dynamics Laboratory (GFDL)	GFDL-CM4	r1i1p1f1	v20180701	yes	10–12
Centre National de Recherches Météorologi ques (CNRM)***	CNRM- ESM2-1	r1i1p1f2	v20191021	no	13–15
Beijing Climate Center (BCC)	BCC-CSM2- MR	r1i1p1f1	v20190314	no	16–18
EC-Earth- Consortium***	EC-Earth3- Veg	r2i1p1f1	v20200226	yes	19–21
Met Office Hadley Centre (MOHC)	UKESM1-0- LL	r2i1p1f2	v20190507	yes	22–24

Institute for Numerical Mathematics (INM) ^{***}	INM-CM4-8	r1i1p1f1	v20190603	no	25–27
Chinese Academy of Meteorologica l Sciences (CAMS) ^{***}	CAMS- CSM1-0	r2i1p1f1	v20190924	yes	28–30
National Center for Atmospheric Research (NCAR) ^{***}	CESM2	r4i1p1f1	v20200528	yes	31–33
Commonweal th Scientific and Industrial Research Organisation (CSIRO) ^{**}	ACCESS- ESM1-5	r1i1p1f1	v20191115	yes	34–36
Fondazione Centro Euro- Mediterraneo sui Cambiamenti (CMCC) ^{***}	CMCC-CM2- SR5	r1i1p1f1	v20200622	yes	37–39

Research Center for Environmental Changes (AS-RCEC)***	TaiESM1	r1i1p1f1	v20200901	no	40–42
--	---------	----------	-----------	----	-------

248

249 **Supplementary table 4: Indicates which predictors have been applied for which figures.**

250 From which models the predictors are available can be found in Table 3. *S denotes a

251 Supplementary figure.

Predictors	Used for Figure*
Surface net radiation, soil moisture, terrestrial evaporation, Leaf Area Index, Aridity Index	4, S12-14
Crop & tree fraction	S13

252

253 References

254 1. Wickham, H. *et al.* *ggplot2: Create Elegant Data Visualisations Using the Grammar of*
 255 *Graphics*. (2022).

256 2. Bivand, R. *et al.* *maptools: Tools for Handling Spatial Objects*. (2022).

257 3. Lofgren, B. M., Hunter, T. S. & Wilbarger, J. Effects of using air temperature as a proxy
 258 for potential evapotranspiration in climate change scenarios of Great Lakes basin
 259 hydrology. *Journal of Great Lakes Research* **37**, 744–752 (2011).

260 4. Milly, P. C. D. & Dunne, K. A. Potential evapotranspiration and continental drying. *Nature*
 261 *Clim Change* **6**, 946–949 (2016).

- 262 5. Maes, W. H., Gentine, P., Verhoest, N. E. C. & Miralles, D. G. Potential evaporation at
263 eddy-covariance sites across the globe. *Hydrology and Earth System Sciences* **23**, 925–948
264 (2019).
- 265 6. Clapp, R. B. & Hornberger, G. M. Empirical equations for some soil hydraulic properties.
266 *Water Resources Research* **14**, 601–604 (1978).
- 267 7. Buitink, J., Melsen, L. A. & Teuling, A. J. Seasonal discharge response to temperature-
268 driven changes in evaporation and snow processes in the Rhine Basin. *Earth System*
269 *Dynamics* **12**, 387–400 (2021).
- 270 8. Hersbach, H. *et al.* The ERA5 global reanalysis. *Quarterly Journal of the Royal*
271 *Meteorological Society* **146**, 1999–2049 (2020).
- 272 9. Hersbach, H. *et al.* ERA5 monthly averaged data on single levels from 1979 to present.
273 (2019) doi:10.24381/CDS.F17050D7.
- 274 10. Held, I. M. *et al.* Structure and Performance of GFDL’s CM4.0 Climate Model. *Journal of*
275 *Advances in Modeling Earth Systems* **11**, 3691–3727 (2019).
- 276 11. Guo, H. *et al.* NOAA-GFDL GFDL-CM4 model output historical. (2018)
277 doi:10.22033/ESGF/CMIP6.8594.
- 278 12. Guo, H. *et al.* NOAA-GFDL GFDL-CM4 model output prepared for CMIP6 ScenarioMIP.
279 (2018) doi:10.22033/ESGF/CMIP6.9242.
- 280 13. Seferian, R. CNRM-CERFACS CNRM-ESM2-1 model output prepared for CMIP6 CMIP
281 historical. (2018) doi:10.22033/ESGF/CMIP6.4068.
- 282 14. Séférian, R. *et al.* Evaluation of CNRM Earth System Model, CNRM-ESM2-1: Role of
283 Earth System Processes in Present-Day and Future Climate. *Journal of Advances in*
284 *Modeling Earth Systems* **11**, 4182–4227 (2019).
- 285 15. Voldoire, A. CNRM-CERFACS CNRM-ESM2-1 model output prepared for CMIP6
286 ScenarioMIP ssp585. (2019) doi:10.22033/ESGF/CMIP6.4226.

- 287 16. Wu, T. *et al.* The Beijing Climate Center Climate System Model (BCC-CSM): the main
288 progress from CMIP5 to CMIP6. *Geoscientific Model Development* **12**, 1573–1600 (2019).
- 289 17. Wu, T. *et al.* BCC BCC-CSM2MR model output prepared for CMIP6 CMIP historical.
290 (2018) doi:10.22033/ESGF/CMIP6.2948.
- 291 18. Xin, X. *et al.* BCC BCC-CSM2MR model output prepared for CMIP6 ScenarioMIP
292 ssp370. (2019) doi:10.22033/ESGF/CMIP6.3035.
- 293 19. Consortium (EC-Earth), E.-E. EC-Earth-Consortium EC-Earth3-Veg-LR model output
294 prepared for CMIP6 CMIP historical. (2020) doi:10.22033/ESGF/CMIP6.4707.
- 295 20. Consortium (EC-Earth), E.-E. EC-Earth-Consortium EC-Earth3-Veg model output
296 prepared for CMIP6 ScenarioMIP. (2019) doi:10.22033/ESGF/CMIP6.727.
- 297 21. Döscher, R. *et al.* The EC-Earth3 Earth System Model for the Climate Model
298 Intercomparison Project 6. *Geoscientific Model Development Discussions* 1–90 (2021)
299 doi:10.5194/gmd-2020-446.
- 300 22. Good, P. *et al.* MOHC UKESM1.0-LL model output prepared for CMIP6 ScenarioMIP.
301 (2019) doi:10.22033/ESGF/CMIP6.1567.
- 302 23. Tang, Y. *et al.* MOHC UKESM1.0-LL model output prepared for CMIP6 CMIP historical.
303 (2019) doi:10.22033/ESGF/CMIP6.6113.
- 304 24. Sellar, A. A. *et al.* UKESM1: Description and Evaluation of the U.K. Earth System Model.
305 *Journal of Advances in Modeling Earth Systems* **11**, 4513–4558 (2019).
- 306 25. Volodin, E. M. *et al.* Simulation of the modern climate using the INM-CM48 climate
307 model. *Russian Journal of Numerical Analysis and Mathematical Modelling* **33**, 367–374
308 (2018).
- 309 26. Volodin, E. *et al.* INM INM-CM4-8 model output prepared for CMIP6 CMIP historical.
310 (2019) doi:10.22033/ESGF/CMIP6.5069.

- 311 27. Volodin, E. *et al.* INM INM-CM4-8 model output prepared for CMIP6 ScenarioMIP.
312 (2019) doi:10.22033/ESGF/CMIP6.12321.
- 313 28. Rong, X. CAMS CAMS_CSM1.0 model output prepared for CMIP6 CMIP historical.
314 (2019) doi:10.22033/ESGF/CMIP6.9754.
- 315 29. Rong, X. CAMS CAMS-CSM1.0 model output prepared for CMIP6 ScenarioMIP. (2019)
316 doi:10.22033/ESGF/CMIP6.11004.
- 317 30. Rong, X.-Y. *et al.* Introduction of CAMS-CSM model and its participation in CMIP6.
318 *Advances in Climate Change Research* **15**, 540 (2019).
- 319 31. Danabasoglu, G. NCAR CESM2 model output prepared for CMIP6 CMIP historical.
320 (2019) doi:10.22033/ESGF/CMIP6.7627.
- 321 32. Danabasoglu, G. NCAR CESM2 model output prepared for CMIP6 ScenarioMIP ssp585.
322 (2019) doi:10.22033/ESGF/CMIP6.7768.
- 323 33. Danabasoglu, G. *et al.* The Community Earth System Model Version 2 (CESM2). *Journal*
324 *of Advances in Modeling Earth Systems* **12**, e2019MS001916 (2020).
- 325 34. Ziehn, T. *et al.* The Australian Earth System Model: ACCESS-ESM1.5. *JSHESS* **70**, 193–
326 214 (2020).
- 327 35. Ziehn, T. *et al.* CSIRO ACCESS-ESM1.5 model output prepared for CMIP6 CMIP
328 historical. (2019) doi:10.22033/ESGF/CMIP6.4272.
- 329 36. Ziehn, T. *et al.* CSIRO ACCESS-ESM1.5 model output prepared for CMIP6 ScenarioMIP
330 ssp585. (2019) doi:10.22033/ESGF/CMIP6.4333.
- 331 37. Cherchi, A. *et al.* Global Mean Climate and Main Patterns of Variability in the CMCC-
332 CM2 Coupled Model. *Journal of Advances in Modeling Earth Systems* **11**, 185–209 (2019).
- 333 38. Lovato, T. & Peano, D. CMCC CMCC-CM2-SR5 model output prepared for CMIP6 CMIP
334 historical. (2020) doi:10.22033/ESGF/CMIP6.3825.

- 335 39. Lovato, T. & Peano, D. CMCC CMCC-CM2-SR5 model output prepared for CMIP6
336 ScenarioMIP. (2020) doi:10.22033/ESGF/CMIP6.1365.
- 337 40. Lee, W.-L. & Liang, H.-C. AS-RCEC TaiESM1.0 model output prepared for CMIP6 CMIP
338 historical. (2020) doi:10.22033/ESGF/CMIP6.9755.
- 339 41. Lee, W.-L. & Liang, H.-C. AS-RCEC TaiESM1.0 model output prepared for CMIP6 CMIP.
340 (2019) doi:10.22033/ESGF/CMIP6.9684.
- 341 42. Lee, W.-L. *et al.* Taiwan Earth System Model Version 1: description and evaluation of
342 mean state. *Geoscientific Model Development* **13**, 3887–3904 (2020).
- 343